Sub-Module Voltage Selection for an 800 V DC Bus Equivalent CHB-BESS based EV Powertrain Design

Rishab Anand*, Peng Han*, Alex Q. Huang* and Vincent Molina†
*Semiconductor Power Electronics Center, The University of Texas at Austin, Austin, TX, USA.
†BMW of North America, LLC, Mountain View, CA, USA.
Email: rishab.anand@utexas.edu

2024 IEEE Transportation Electrification Conference and Expo (ITEC) | 979-8-3503-1766-4/24/$31.00 ©2024 IEEE | DOI: 10.1109/ITEC60657.2024.10598837

***Abstract*—A method to optimally select sub-module (SM) voltage for a cascaded H-bridge (CHB) battery energy storage system (BESS) using Si MOSFETs has been presented. Design of an 800 V DC equivalent EV powertrain has been used as an illustrative example. The method takes into account converter efficiency and bill of materials (BoM) cost. Battery capacity and power utilization is also considered. Among devices with the same drain-source breakdown voltage (BV) rating (corresponding to the choice of the SM voltage), a cost times device on-state resistance figure-of-merit (FoM) has been proposed to select the optimal device. Between these devices with different BV ratings, this FoM displays a generally decreasing trend with increasing BV rating. However, at device BV ratings greater than 100 V, a relatively large (and somewhat impractical) number of devices are required to be connected in parallel to meet the conduction loss target alone. Along with the large switching frequency due to the reduced number of available output voltage levels, this raises the switching losses to a level wherein a high efficiency target ($\geq 99\%$) cannot be met. Statistically, battery utilization has been shown to change insignificantly with the choice of the SM voltage. As an unintended consequence of distributing battery cells into three separate phase strings, the likelihood of encountering a lower battery capacity than expected from the scaled cell capacity is in fact shown to increase.**

***Index Terms*—Cascaded H-bridge, battery energy storage, electric vehicles, inverter, Li-ion battery**

I. Introduction

The demand for ultrafast charging has been driving a move towards 800 V EV powertrain architectures [1]. Further, higher voltage architectures are inherently preferred over conventional 400 V architecture for heavy duty vehicle electrification [1]. Similarly, the proliferation of stationary battery energy storage across a wide range of application areas is driving the need for modularity, reusability and lower costs [2]. In both of these applications, the cascaded H-bridge (CHB) converter with batteries embedded within the individual sub-modules (SMs) utilizing Si MOSFETs can potentially outperform typical 2-level architectures using 1200V Si IGBTs or SiC MOSFETs in terms of efficiency, while bringing in additional benefits such as reduced volumetric iron and ac copper loss in the electrical machine [3], improved battery utilization and reliability [4], opportunity for simpler and more robust auxiliary power unit designs [5] to list a few.

This work was partially funded by the NSF under PFI-RP Award 2234618 and by the U.S. Department of Energy EcoCAR EV Challenge.

The sub-module voltage in a CHB converter is a fundamental design choice that governs key metrics such as the output voltage harmonic spectrum, converter efficiency and cost. For the embedded battery modules, this governs the achievable improvement in capacity and power utilization. Howerever, a comprehensive method for selection of this key parameter has been lacking in the literature. Some existing designs target medium voltage applications, wherein the primary intent is to demonstrate operation at voltages beyond the blocking voltage of any single switching device, and hence implicitly use devices with the highest available BV rating [6], [7]. Other designs tend to chose the SM voltage rating around available battery module voltage ratings [8].

Using the design of an 800 V DC bus equivalent CHB-BESS, this article illustrates a method to optimally select SM voltage rating. Converter efficiency and cost are addressed in Section II. Battery capacity and power utilization is addressed in Section III. Section IV concludes this article.

II. Converter Efficiency and Cost Tradeoff

Fig. 1 shows the structure of the proposed CHB-BESS. $N_{p,cells}$ cells are connected in parallel to form bricks, of which $N_{s,bricks}$ are then connected in series to form battery modules. These battery modules are connected to the DC side of H-bridge power stages to realize H-bridge SMs. A series-connection of these SMs is used to realize a phase leg which are in-turn connected in a star configuration to realize the 3-phase CHB-BESS. The CHB-BESS does not have a DC link and the motor is directly connected to the three phase leg outputs.

In a 2-level inverter, the minimum DC bus voltage is determined by the required peak value of the line-to-line voltage at the output. This in-turn determines the number of battery cells required to be connected in series. In a CHB-BESS, the same constraint determines the total number of series-connected battery cells across all SMs in any phase leg. However, the number of SMs per phase leg N_{mod} and subsequently the number of battery cells within each SM is a design choice. Table I lists all possible configurations for an 80 kWh, 800 V DC equivalent CHB-BESS built using 5 Ah Li-NMC cells. The cells are limited to a maximum terminal voltage of

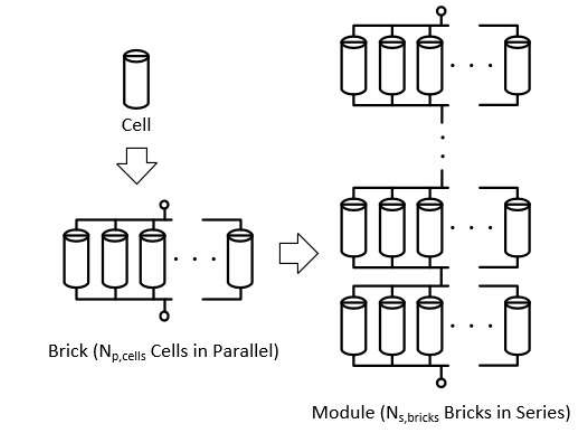

(a) Battery Module Structure and Terminology

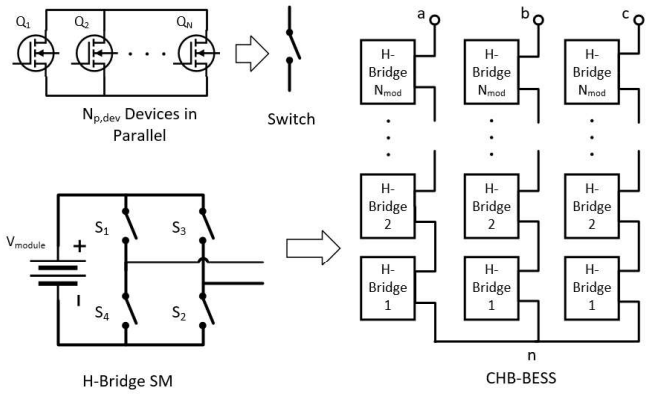

(b) 3-phase Y-connected CHB Inverter Structure and Terminology

Fig. 1: CHB-BESS System Structure and Terminology

4.2 V (corresponding to the fully charged state). The drain-source BV rating of the device chosen to realize the H-bridge switches determines the maximum battery module voltage and subsequently the number of series-connected bricks in each SM and the number of SMs in each phase. The on-state resistance of the device $R_{on,dev}$ is related to its BV, so that it is undesirable to leave excessive margins between the maximum battery module voltage and the device BV. For simplicity, the CHB-BESS is assumed to be driving a purely resistive load. To reduce conduction loss, each of the four switches within the H-bridge may be realized through a parallel connection of $N_{p,dev}$ individual switching devices. This may also be driven by cooling constraints limiting allowable heat generation. The total conduction power loss in the CHB-BESS is given by (1). The total switching power loss is given by (2).

$$P_{loss,cond} = 3N_{mod}\left[2I_{rms}^2\left(\frac{R_{on,dev}}{N_{p,dev}}\right)\right] \tag{1}$$

$$P_{loss,sw} = 3N_{mod}\Big[4N_{p,dev}\Big\{V_{mod}\frac{I_d}{N_{p,dev}}\left(t_{on}+t_{off}\right) + C_{oss}V_{mod}^2 + V_{mod}Q_{rr}\Big\}\Big]f_s \tag{2}$$

The temperature dependence of device on-state resistance $R_{on,dev}$ is factored into the loss calculations. In general, the device choice is driven by the desire to meet the loss targets at the lowest cost. The BoM cost for the CHB-BESS system is given by (3). The balance BoM cost per SM excluding the device cost should be nearly constant across all design choices and was estimated to be approximately 80 USD. Perturbing this estimate did not change the trend in the results. As a result of a large number of output voltage levels, the CHB is able to operate at a reduced switching frequency [9], keeping switching losses in check so that conduction losses dominate. The figure of merit (FoM) of interest proposed is therefore the product of the CHB-BESS conduction loss and the system cost and is given by (4).

$$Cost_{CHB} = 3N_{mod}\left(4N_{p,dev}Cost_{dev} + Cost_{balance}\right) \tag{3}$$

$$FoM = P_{loss}Cost = 72N_{mod}^2 I_{rms}^2 R_{on,dev}\left(Cost_{dev} + \frac{Cost_{balance}}{4N_{p,dev}}\right) \tag{4}$$

Over a comprehensive database of commercially available devices [10], this FoM was used to select the best device among each set of devices with the same drain-source breakdown voltage rating. Table I also lists the device part number, the device parallel count required to reach an efficiency greater than 99% and the FoM value for the best-suited devices. Between these devices with different breakdown voltage ratings, this FoM displays a generally decreasing trend with increasing BV rating. As is expected, designs with large SM counts simply end up being prohibitively expensive due to large component counts. If the conduction losses alone were to be considered, it is always more cost effective to use designs with high SM voltages and low SM counts while paralleling large enough number of devices to meet loss targets.

Table I also lists the switching frequencies that the designs must operate at to achieve similar output voltage harmonic spectrum as a 2-level inverter operating at 20 kHz [9]. The total switching losses, including overlap, C_{oss} and reverse recovery, as a fraction of the conduction loss have also been tabulated. Due to the higher switching frequency and also in part due to the large number of parallel-connected devices required to meet the conduction loss target alone, using devices with BV of 150 V or higher, the switching losses add up to a significant value so that it is no longer possible to achieve the overall loss target. The well-known phase-shifted PWM scheme was used for the control, although the trend is expected remain unchanged with a different modulation scheme. The same is expected with regards to assumptions made regarding the device current waveform and the device turn-on and turn-off durations.

It is therefore concluded that using devices with BV between 80 to 100 V (with 14 to 16 cells in series per SM), provides the best trade-off in terms of CHB-BESS cost and efficiency.

Structure	V_{BV} (V)	Pack Config.	V_{SM} (V)	N_{mod}	F_s (Hz)	Device P/N	$N_{p,dev}$	FoM (\$ kW)	$\frac{P_{sw}}{P_{cond}}$
2-Level	1200	22P 192S	806.4	-	20000	-	-	-	
CHB	20	13P 3S	12.6	37	540	SISS80DN-T1-GE3	5	19862	0.03
	30	13P 5S	21	22	900	IQDH35N03LM5ATMA1	2	6778	0.09
	40	13P 7S	29.4	16	1250	IAUCN04S7N004ATMA1	2	4389	0.14
	60	13P 10S	42	11	1820	NTMTS0D7N06CTXG	2	3840	0.19
	80	13P 14S	58.8	8	2500	IAUT300N08S5N011ATMA1	2	3024	0.22
	100	13P 16S	67.2	7	2860	IAUT300N10S5N014ATMA1	2	3045	0.23
	120	13P 18S	75.6	6	3330	IPT030N12N3GATMA1	3	3288	0.23
	150	13P 22S	92.4	5	4000	NVMTSC4D3N15MC	4	2956	0.30
	200	13P 28S	117.6	4	5000	SUM90100E-GE3	7	2869	0.40

TABLE I: Possible configurations for an 80 kWh, 800 V DC equivalent CHB-BESS using 5 Ah Li-NMC cells

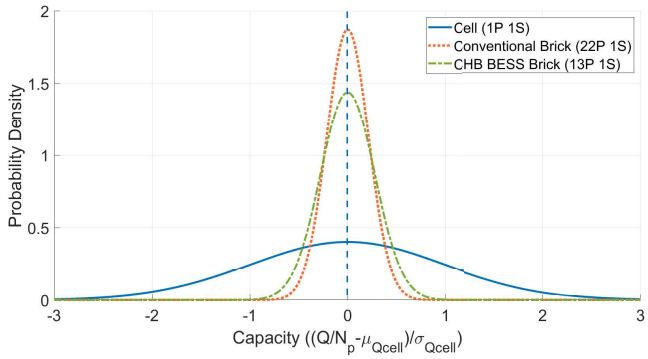

(a) Capacity distribution for single cells compared to 22P (2-level) and 13P (CHB-BESS) bricks

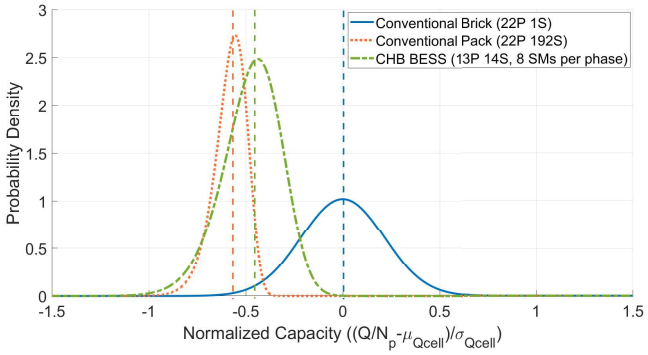

(b) Capacity distribution for conventional packs (22P 192S) compared to CHB-BESS (13P 14S, 8 SMs per phase)

Fig. 2: Comparison of capacity PDF across different BESS system components and designs. The dashed vertical lines represent the mean values of the corresponding distribution.

III. Battery Utilization

The usable capacity of a battery pack is limited by its constituent series-connected brick with the lowest capacity. Similarly the peak power capability is also limited by the brick with the highest resistance [11]. When connecting a larger number of bricks in series, it is more likely to encounter bricks with lower capacity or higher impedance [12]. It could be therefore expected that the loss in usable pack capacity and peak power capability will be larger for an 800 V pack comprising a larger number of series-connected bricks vis-a-vis a smaller voltage pack [12].

The CHB-BESS structure breaks down a larger battery pack into smaller modules. Each of these can then be fully utilized without any impact from weaker cells in other modules, thus potentially overcoming some of the usable capacity and power loss [8]. However, a larger number of these small SMs although desirable, comes with increased cost and control complexity. It is therefore important to obtain quantitative metrics on capacity loss in battery packs arising from cell level dissimilarities.

Consecutive combination of deviations in each of the many cell manufacturing process steps can be assumed to render cell capacity as normally distributed with mean μ_Q and variance σ_Q^2 [12]. This is captured in (5). For a worst case analysis, the effect of capacity-based binning has been ignored.

$$Q_{cell} \sim \mathcal{N}(\mu_Q, \sigma_Q^2) \tag{5}$$

A brick is made up of N_p cells connected in parallel so that the brick capacity Q_{brick} can be computed as the sum of the constituent cell capacities, as shown in (6). The cell capacities are all independent identically distributed (IID) random variables. The brick capacity would therefore again be a normally distributed random variable, but with mean $N_p\mu_Q$ and variance $N_p\sigma_Q^2$ as is shown in (7) [12].

$$Q_{brick} = \sum_{i=1}^{N_p} Q_{cell,i} \tag{6}$$

$$Q_{brick} \sim \mathcal{N}(N_p\mu_Q, N_p\sigma_Q^2) \tag{7}$$

The ratio of the normalized capacity standard deviation (capacity standard distribution divided by the respective mean capacity) for an individual cell and a brick comprising N_p cells in parallel is shown in (8).

$$\frac{\sigma_{Q,brick}}{\mu_{Q,brick}} = \frac{1}{\sqrt{N_p}} \frac{\sigma_Q}{\mu_Q} \tag{8}$$

It can be seen that the normalized standard deviation for a brick is smaller than that of a cell by a factor $\sqrt{N_p}$. The probability density functions (PDFs) for cell capacity, that of a 22P brick in a conventional pack and of a 13P brick in a CHB-BESS SM are plotted in Fig. 2(a). The cell capacity is assumed to have a mean value of 5 Ah with a tolerance (3σ) of 5%. This is a conservative estimate and state- of-the-art cell manufacturing processes typically yield highly

consistent cells with much less variance. It can be seen that the capacities of the 22P brick are expected to be far more consistent than a single cell. This is due to differences in cell capacities being averaged out during parallel connection [12]. More importantly, for CHB-BESS, the need to distribute cells into three phases forces the use of a smaller brick whose capacity is expected to be less consistent than a brick intended for a conventional pack.

Without any redistributive active balancing, pack capacity Q_{pack} would simply be the minimum of constituent N_s brick capacities [11]. This is expressed in (9). The PDF of the pack capacity $f_{Q_{pack}}$ can be computed by first computing the cumulative density function (CDF) $F_{Q_{pack}}$ and is shown in (10). The CDF of the pack capacity can be computed from the CDF of the brick capacity $F_{Q_{brick}}$ and is shown in (11).

$$Q_{pack} = \min_{i=1\ldots N_s} Q_{brick,i} \tag{9}$$

$$f_{Q_{pack}}(q) = N_s f_{Q_{brick}}(q) \left[1 - F_{Q_{pack}}(q)\right]^{N_s-1} \tag{10}$$

$$F_{Q_{pack}}(q) = 1 - \left[1 - F_{Q_{brick}}(q)\right]^{N_S} \tag{11}$$

A CHB-BESS can be controlled to load constituent SMs in proportion to the capacity of the corresponding embedded battery modules and therefore utilize the entire available capacity across all SMs [8]. The system capacity is therefore the mean value of the capacities of these embedded battery modules. The PDF for these battery module capacities can be computed using (7) and (10) for any configuration chosen from Table I. Since the battery module capacities are IID random variables, the system capacity (which is the mean of these RVs) can be shown to have the same distribution as these module capacities.

The probability density function for pack capacity for a conventional 800 V battery pack and that of a CHB-BESS is shown in Fig. 2(b). The PDF of the capacity for the 22P brick has been included for reference. It can be observed that the mean capacity for CHB-BESS systems is only very marginally better than the mean capacity for a conventional battery pack. In fact, the tail for the CHB-BESS distribution spreads further left than the conventional packs, indicating a larger likelihood to obtain packs with low capacity. As the SM size becomes smaller and the SM count increases, the mean value will approach that of the individual brick. Most importantly, the achievable improvement is less than the SoC estimation accuracy achievable with the current generation of battery management systems [11]. The system controller relies on SoC estimates to achieve full capacity utilization. It can therefore be concluded that battery pack capacity utilization is not a significant metric for CHB-BESS SM size selection when using new batteries with small cylindrical cells. Similar conclusions can be drawn for the difference in brick impedance (causing deterioration in battery pack power availability) and brick self-discharge rates across a battery system.

IV. Conclusion

Given an efficiency target, the proposed methodology enables selection of a switching device that can meet the target at the lowest cost. Using a smaller number of submodules with higher battery voltages is preferred due to a lower cost, till the point wherein it is simply no longer possible to meet the efficiency target due to combination of large number of parallel-connected devices and higher switching frequencies causing the switching loss to become very high. For systems utilizing small cylindrical cells, battery utilization is not a dominant factor in the choice of submodule voltage. Battery pack mean useable capacity, brick impedance mismatch and self-discharge rate difference is not significantly improved by distributing the cells into CHB-RESS submodules. Distributing the battery across the three phase strings forces the use of bricks with smaller number of cells connected in parallel which increases the likelihood of encountering bricks with lower capacity. The conclusions may differ if large format cells are used, reducing the parallel-connected cell count.

References

[1] I. Aghabali, J. Bauman, P. J. Kollmeyer, Y. Wang, B. Bilgin, and A. Emadi, "800-v electric vehicle powertrains: Review and analysis of benefits, challenges, and future trends," *IEEE Transactions on Transportation Electrification*, vol. 7, no. 3, pp. 927–948, 2021.

[2] G. Wang, G. Konstantinou, C. D. Townsend, J. Pou, S. Vazquez, G. D. Demetriades, and V. G. Agelidis, "A review of power electronics for grid connection of utility-scale battery energy storage systems," *IEEE Transactions on Sustainable Energy*, vol. 7, no. 4, pp. 1778–1790, 2016.

[3] L. Chang, T. M. Jahns, and R. Blissenbach, "Estimation of pwm-induced iron loss in ipm machines incorporating the impact of flux ripple waveshape and nonlinear magnetic characteristics," *IEEE Transactions on Industry Applications*, vol. 56, no. 2, pp. 1332–1345, 2020.

[4] Z. Liu, C. Tan, and F. Leng, "A reliability-based design concept for lithium-ion battery pack in electric vehicles," *Reliability Engineering System Safety*, vol. 134, pp. 169–177, 2015.

[5] C. Wang, P. Zheng, and J. Bauman, "A review of electric vehicle auxiliary power modules: Challenges, topologies, and future trends," *IEEE Transactions on Power Electronics*, vol. 38, no. 9, pp. 11 233–11 244, 2023.

[6] J. I. Y. Ota, T. Sato, and H. Akagi, "Enhancement of performance, availability, and flexibility of a battery energy storage system based on a modular multilevel cascaded converter (mmcc-ssbc)," *IEEE Transactions on Power Electronics*, vol. 31, no. 4, pp. 2791–2799, 2016.

[7] M. Barresi, D. De Simone, R. Barzaghi, S. C. Dezza, L. Meraldi, D. Rosati, and L. Piegari, "Optimal components selection for a dab model of chb converter," *IEEE Journal of Emerging and Selected Topics in Industrial Electronics*, vol. 4, no. 3, pp. 802–817, 2023.

[8] G. Liang, E. Rodriguez, G. G. Farivar, E. Nunes, G. Konstantinou, C. D. Townsend, R. Leyva, and J. Pou, "Model predictive control for inter-submodule state-of-charge balancing in cascaded h-bridge converter-based battery energy storage systems," *IEEE Transactions on Industrial Electronics*, pp. 1–10, 2023.

[9] Y. Li, Y. Wang, and B. Q. Li, "Generalized theory of phase-shifted carrier pwm for cascaded h-bridge converters and modular multilevel converters," *IEEE Journal of Emerging and Selected Topics in Power Electronics*, vol. 4, no. 2, pp. 589–605, 2016.

[10] Digikey, ""N-Channel MOSFET (Metal Oxide) Single FETs, MOSFETs"," *Digikey*, 2023. [Online]. Available: https://www.digikey.com/en/products/filter/transistors/fets-mosfets/single-fets-mosfets/278 (accessed: 22.12.2023)

[11] G. L. Plett, *Battery Management Systems, Vol.2: Eqvt. Circuit Methods*. Artech House, 2015.

[12] A. Abdellahi, S. Atalay, and A. Rajan, "Impact of cell variability on pack statistics for different vehicle segments," *Journal of Power Sources*, vol. 508, p. 230246, 2021.